Available online at www.sciencedirect.com
ScienceDirect
Journal of Power Sources 179 (2008) 106–112
JOURNAL OF POWER SOURCES
www.elsevier.com/locate/jpowsour

Thermophysical properties and devitrification of $SrO–La_2O_3–Al_2O_3–B_2O_3–SiO_2$-based glass sealant for solid oxide fuel/electrolyzer cells

M.K. Mahapatra, K. Lu *, W.T. Reynolds Jr.

Department of Materials Science and Engineering, Virginia Polytechnic Institute and State University, Blacksburg, VA 24061, USA

Received 26 November 2007; received in revised form 28 December 2007; accepted 31 December 2007
Available online 6 January 2008

Abstract

Thermal behaviors and stability of glass/glass–ceramic-based sealant materials are critical issues for high temperature solid oxide fuel/electrolyzer cells. To understand the thermophysical properties and devitrification behavior of $SrO–La_2O_3–Al_2O_3–B_2O_3–SiO_2$ system, glasses were synthesized by quenching $(25 - X)SrO–20La_2O_3–(7 + X)Al_2O_3–40B_2O_3–8SiO_2$ oxides, where X was varied from 0.0 mol% to 10.0 mol% at 2.5 mol% interval. Thermal properties were characterized by dilatometry and differential scanning calorimetry (DSC). Microstructural studies were performed by scanning electron microscopy (SEM), energy dispersive spectroscopy (EDS), and X-ray diffraction (XRD). All the compositions have a glass transition temperature greater than 620 °C and a crystallization temperature greater than 826 °C. Also, all the glasses have a coefficient of thermal expansion (CTE) between $9.0 \times 10^{-6}\ K^{-1}$ and $14.5 \times 10^{6}\ K^{-1}$ after the first thermal cycle. La_2O_3 and B_2O_3 contribute to glass devitrification by forming crystalline $LaBO_3$. Al_2O_3 stabilizes the glasses by suppressing devitrification. Significant improvement in devitrification resistance is observed as X increases from 0.0 mol% to 10.0 mol%.

Keywords: Glass transition temperature; Thermal expansion coefficient; Dilatometric softening point; Devitrification; Microstructure

1. Introduction

Solid oxide fuel cells (SOFC) convert chemical energy into electrical energy using hydrogen or hydrocarbon as fuel. When a SOFC is used in a reverse manner, a clean synthetic fuel such as hydrogen can be generated by splitting water/steam at high temperatures, and such cells are called solid oxide electrolyzer cells (SOEC). As an alternative for clean power and hydrogen generation, solid oxide cells (both SOFC and SOEC) have attracted great attraction [1]. Currently, the preferred SOFC/SOEC designs are planar mode. While the planar design offers high energy/fuel generation efficiency, it also requires stable, gas-tight seals to prevent mixing of fuel gas and oxygen at high temperatures [2–4]. A lack of suitable high temperature seals hinders long-term reliability and durability of planar SOFC and SOEC [5,6].

Glass and glass–ceramic viscous sealant materials are most promising in fulfilling SOFC/SOEC requirements due to their superior thermophysical properties than metals, metal–ceramic composites, and compressive seals [7]. To be used as a SOFC/SOEC seal, glass and glass–ceramic have to meet the following criteria. Coefficient of thermal expansion (CTE) should be greater than $9.0 \times 10^{-6}\ K^{-1}$ in order to match with other cell components, such as zirconia, stainless steel, and lanthanum manganate. Glass transition temperature (T_g) should be less than the cell operating temperatures (800–900 °C), and glass softening temperature (T_d) should be high enough to avoid excessive glass flow at cell operation temperatures. Also, continuous and/or excessive devitrification of glass or glass–ceramic sealant should not occur; this requires that glass crystallization temperature (T_c) be much higher than the cell operation temperatures. Chemical stability and interfacial compatibility with other cell components should be sufficient to sustain reducing

* Corresponding author. Tel.: +1 540 231 3225; fax: +1 540 231 8919.
E-mail addresses: mkmanoj@vt.edu (M.K. Mahapatra), klu@vt.edu (K. Lu), reynolds@vt.edu (W.T. Reynolds Jr.).

0378-7753/$ – see front matter © 2008 Elsevier B.V. All rights reserved.
doi:10.1016/j.jpowsour.2007.12.101

and oxidizing atmospheres at high temperatures for long periods of time (such as 40,000 h) without failure. In addition to the above demands, sealant must be electrically insulating.

Several glasses and glass–ceramics have been studied as solid oxide cell seals [7,8]. Among them, BaO containing sealants are the mostly reported one. For BaO containing sealants, the main disadvantages arise from deleterious interfacial reactions with other cell components (such as interconnect) and formation of celsian ($BaAl_2Si_2O_8$) and its polymorph hexacelsian crystalline phases. Both phases have low CTE. Also, the difference between the CTE values of celsian phase ($2.29 \times 10^{-6}\,K^{-1}$) and hexacelcian phase ($8.0 \times 10^{-6}\,K^{-1}$) develops thermal stress and degrades performance [9,10]. Because of these shortcomings, there is a need to search new glass or glass–ceramic systems as sealant materials.

A new composition based on lanthanum–aluminium–alkaline earth borosilicate system has been reported [11,12]. In this system, B_2O_3 and SiO_2 act as glass formers, La_2O_3 modifies viscosity [11], SrO modifies CTE [13], and Al_2O_3 retards devitrification [14]. Even though prior studies indicate that such glass system has desirable thermophysical properties [11,12], there have been conflicting reports on the T_g and CTE values. Also, the glass stability of this system has not been assessed.

To explore the potential of the lanthanum–aluminium–alkaline earth borosilicate system as a SOFC/SOEC sealant, this work focuses on the effect of SrO and Al_2O_3 contents and thermal cycling on the devitrification behavior and thermophysical properties of the glass system. The stability and microstructural evolution of different glass compositions are evaluated. The study also suggests strategies for further optimization of the sealant glass composition.

2. Experimental procedure

2.1. Preparation of glass

Glass samples were prepared based on $(25-X)$SrO–$20La_2O_3$–$(7+X)Al_2O_3$–$40B_2O_3$–$8SiO_2$ compositions, where X was varied from 0.0 mol% to 10.0 mol% at 2.5 mol% interval. The base composition was reported in the literature [11]. The corresponding oxide powders were ball milled for 5 h. The mixed powders were heated and melted at 1400 °C for 4 h in a box furnace (Lindberg, model no. 51314, Watertown, WI) at 20 °C min^{-1} heating rate before being quenched into a graphite mold.

2.2. Differential scanning calorimetry

Differential scanning calorimetry (DSC) studies were conducted in a simultaneous TG-DTA/DSC apparatus (STA449C/3/G Jupiter, Netzsch Instruments Inc., Burlington, MA). The glass samples were thermally cycled three times at the same heating and cooling rates of 10 °C min^{-1} up to 900 °C and a dwell time of 2 h at 900 °C for thermal behavior analysis. The T_g and T_c temperatures were determined from the DSC data.

2.3. Dilatometry

Softening temperature and CTEs of the glass samples from room temperature to 700 °C were measured with a push rod dilatometer (Model 1600R, The Edward Orton Jr. Ceramic Foundation, OH). This technique also provided another approach of measuring glass transition temperature T_g. The samples were 27 mm in length and 5 mm in diameter. During the dilatometry study, the samples were heated at 3 °C min^{-1} heating rate to 700 °C for 2 h and then cooled to room temperature at 5 °C min^{-1} cooling rate. Each sample was thermally cycled three times under this condition. Linear regression from room temperature to T_g was carried out for each thermal cycle curve to obtain the reported CTEs.

2.4. Microstructural characterization

Microstructural studies were carried out in a field emission scanning electron microscope (SEM) (LEO 1550, Carl Zeiss MicroImaging Inc., Thornwood, NY) for the as-quenched samples and the thermally cycled samples from the DSC experiments. Energy dispersive spectroscopy (EDS) (Helios 600 NanoLab, FEI, Hillsboro, OR) was used to analyse the compositions of the glass phase and the crystalline phase of the samples after the thermal cycling.

2.5. Phase analysis

X-ray diffraction (XRD) studies were carried out in an X'Pert PRO diffractometer (PANalytical B.V., EA Almelo, The Netherlands) to identify the crystalline phases in the thermally cycled samples. The scan rate was 0.0020° s^{-1} with Cu Kα radiation ($\lambda = 1.5406$ Å) and a Ni filter.

3. Results and discussion

3.1. Glass transition and crystallization temperatures

For the studied glass system, the DSC peak temperature was 900 °C. Before 900 °C, there are two heat flow changes on the DSC curves. One is endothermic and the other is exothermic. The endothermic position indicates the glass transition temperature T_g and the exothermic position indicates the crystallization temperature T_c. The T_g and T_c for all the glass compositions are extracted as given in Fig. 1. All the glasses have T_g greater than 620 °C. The effect of increasing Al_2O_3 content on raising T_g is modest and dependent on the Al_2O_3 content. T_g increases by 10 °C as the Al_2O_3 content increases from 7.0 mol% to 17.0 mol%. From Fig. 1, it can also be seen that T_c is 826 ± 1 °C for $X = 0.0$–5.0 mol% and 850 ± 1 °C for $X = 7.5$–10.0 mol%. One important observation is that T_g decreases after the first heating cycle and remains the same for the remaining cycles. This T_g decreases after the first thermal cycle is most likely due to the devitrification of the glass matrix. It also indicates that the remaining glass phase after devitrification has a lower T_g. The change in the composition of the residual glass has been confirmed by EDS and will be discussed later. T_c reflects the

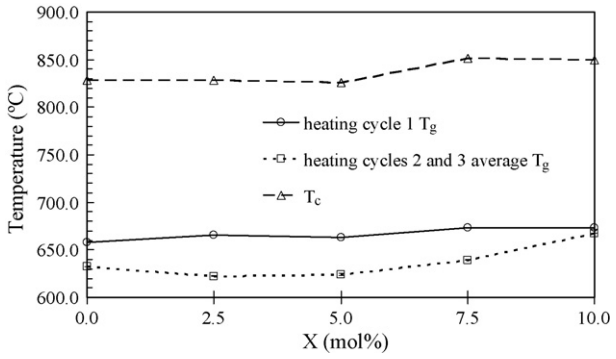

Fig. 1. T_g and T_c change vs. Al_2O_3 content increase (X) from DSC experiments.

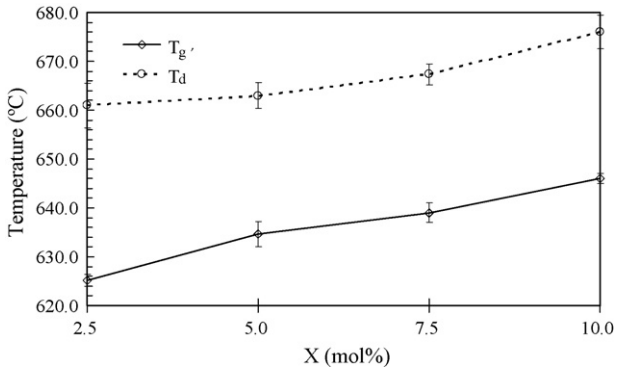

Fig. 3. T_g' and T_d change vs. Al_2O_3 content increase (X) from dilatometry study.

temperature at which some of the glass transforms into one or more crystalline phases and is a direct representation of glass stability. No T_c peaks are observed during the second and the third heating cycles in any of the compositions studied. This indicates that the glasses mainly devitrify during the first heating cycle. This thermally induced phase change is supported by the presence of crystalline/secondary phases in the SEM study.

3.2. Dilatometric softening temperature and thermal expansion coefficient

From the dilatometry study, the dilatometric softening point (T_d), glass transition temperature T_g' (in differentiation from the DSC glass transition temperature T_g), and CTE can be determined. The reading points for the T_d and T_g' are shown in Fig. 2. However, the $(25-X)$SrO–$20La_2O_3$–$(7+X)Al_2O_3$–$40B_2O_3$–$8SiO_2$ glass at $X=0.0$ mol% has very limited glass forming ability. Transparent and crack free dilatometry sample cannot be obtained after six attempts of quenching. Consequently, no thermal expansion data are available for the $X=0.0$ mol% composition. The dilatometry curve for the $(25-X)$SrO–$20La_2O_3$–$(7+X)Al_2O_3$–$40B_2O_3$–$8SiO_2$ glass at $X=2.5$ mol% is shown in Fig. 2 and other compositions show similar trend. T_d and T_g' changes versus Al_2O_3 content increase are shown in Fig. 3.

In Fig. 2, it can be seen that the percent linear change curves shift downwards after each thermal cycle. This is due to a change

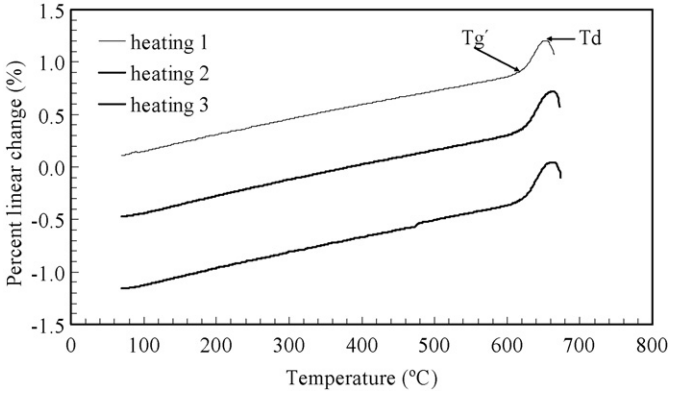

Fig. 2. Percent linear change vs. temperature for the $(25-X)$SrO–$20La_2O_3$–$(7+X)Al_2O_3$–$40B_2O_3$–$8SiO_2$ glass at $X=2.5$ mol% from dilatometry.

in the sample length. Although no visual deformation is observed in the samples after the thermal cycles, the change in the sample dimension, however small it may be, may arise from the deformation of the glass under the compressive load applied by the push rod. This artificially changes the absolute percent linear change value since the initial dimension was used in all the dilatometric calculation.

From Fig. 3, it can be observed that the softening temperature T_d is greater than 660 °C for all the compositions. As X increases from 0.0 mol% to 10.0 mol%, T_d increases from 661 °C to 676 °C. For all the thermal cycles, T_g' and T_d values and the differences between T_g' and T_d are very consistent, differing by less than 40 °C for all the compositions. This suggests that there is no phase separation occurring in the glass during the dilatometry study [15]. After the three thermal cycles, the physical appearance of the samples remains unchanged. This observation also indicates that the glass is stable up to at least 660 °C.

T_g' increases with Al_2O_3 content for all the glass compositions. From $X=2.5$ mol% to $X=10.0$ mol%, T_g' increases by 20 °C. This result is consistent with the DSC results (Fig. 1). However, the value of T_g' obtained from the dilatometry is about 30 °C lower than that from the DSC experiments. The difference between T_g' and T_g from these different experimental methods has been reported [16]. There are two possible reasons for this difference. First, the heating rates are different: 10 °C min^{-1} in the DSC experiment and 3 °C min^{-1} in the dilatometry. This may cause the difference between T_g' and T_g since glass transition temperature is thermal history dependent. Second, T_g' depends on the viscoelastic properties of the glass. In the dilatometry experiment, the samples were subjected to a compressive load by the push rod. This load may affect the viscoelasticity of the glass, shift the T_g' to lower temperatures, and thus cause difference between T_g' and T_g.

CTE decreases with Al_2O_3 content increase X. Also, the CTE during the first thermal cycle is lower than those of the remaining thermal cycles at the temperatures below T_g'. After the first heating cycle, the CTEs remain consistent, demonstrated by the low CTE standard deviation. To illustrate the difference, Fig. 4 shows the CTE changes for the first thermal cycle and the remaining cycles. The CTE values obtained from the first heating cycle are 14.10×10^{-6} K^{-1} at $X=2.5$ mol%, 9.73×10^{-6} K^{-1}

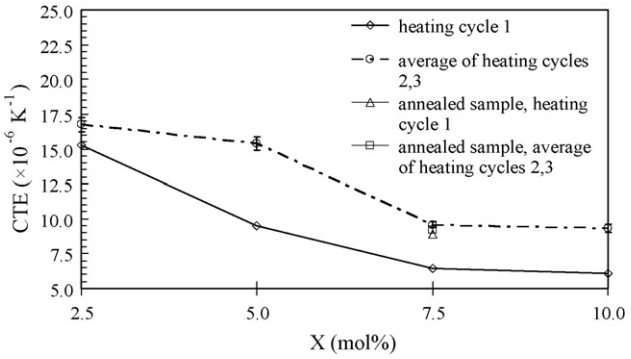

Fig. 4. CTE variation vs. Al_2O_3 content increase (X) from dilatometry.

at $X = 5.0$ mol%, $6.86 \times 10^{-6}\,K^{-1}$ at $X = 7.5$ mol%, and $6.47 \times 10^{-6}\,K^{-1}$ at $X = 10.0$ mol%. Average CTE after the first heating cycle is $16.74 \times 10^{-6}\,K^{-1}$ for $X = 2.5$ mol%, $15.37 \times 10^{-6}\,K^{-1}$ for $X = 5.0$ mol%, $9.58 \times 10^{-6}\,K^{-1}$ for $X = 7.5$ mol%, and $9.30 \times 10^{-6}\,K^{-1}$ for 10.0 mol%. This difference between CTEs between the first and the remaining heating cycles may be explained as follows. The samples used in the dilatometry have been obtained by quenching. Structural rearrangement toward equilibrium glass state is incomplete as the glass melt quickly solidifies. Residual stress is likely to be created during the first thermal cycle. During the dilatometry measurements, the slower heating rate and the peak temperature dwell remove the residual stress in the quenched glass while the peak temperature is low enough to avoid devitrification. Since the cooling rate is also slower, no further thermal stress develops during cooling. Thus after the first heating cycle structural rearrangement of the glass is complete or nearly so. As a result, molar free volume of the sample decreases and CTE increases to a consistent value after the first heating cycle. This prediction is supported by the consistent CTEs in the annealed $(25 - X)SrO–20La_2O_3–(7 + X)Al_2O_3–40B_2O_3–8SiO_2$ sample at $X = 7.5$ mol% (Fig. 4). It should also be noted that there is a sharp CTE decrease when Al_2O_3 content increases (Al_2O_3 has lower CTE than glass). For the as-quenched glass, this happens at lower Al_2O_3 content. For the glass that was thermally cycled once, the glass phase is more stable so the CTE transition happens at slightly higher Al_2O_3 content. This is why the change in CTE at $X = 5.0$ mol% is significantly larger than those at other values.

After the first thermal cycle, the CTEs of all the glass compositions are greater than $9.0 \times 10^{-6}\,K^{-1}$ and show good potential to match with the CTEs of other cell components [17]. Good thermal expansion match with other SOFC/SOEC components such as zirconia electrolyte and stainless steel interconnect [18], moderate T_g, and stability of these compositions make them suitable as sealant materials below 800 °C SOFC/SOEC operation temperatures.

3.3. Microstructural evolution

SEM micrographs of the as-quenched glass samples for all the compositions show absence of crystalline phase or phase separation. The images at the two limits of the studied composition range, $X = 0.0$ mol% and $X = 10.0$ mol%, are shown in Fig. 5. This observation is supported by the XRD patterns to be shown in Fig. 8. The cracks observed in the SEM micrographs were created during SEM sample preparation. This means all the samples studied start with pure glass phase.

The SEM micrographs of the samples after the DSC thermal cycling are given in Fig. 6. The dark phases are glass phase and the bright phases are crystalline phase. There are drastic microstructure differences among glass compositions ranging from $X = 0.0$ mol% to 10 mol%. When the Al_2O_3 content is at $X = 0.0$ mol% (Fig. 6(a)), irregular shaped, equiaxed crystallites appear in the glass matrix. The crystal sizes are about 20 μm. When X increases to 2.5 mol% (Fig. 6(b)), elongated crystallites appear and have a dendritic morphology. Even though the short dimension of these elongated crystallites is less than 20 μm, the long dimension is mostly greater than 20 μm. When X increases to 5.0 mol% (Fig. 6(c)), the crystal phase morphology becomes more needle-shaped. These needles form long strands that are separated by a small amount of glass phase. However, the individual crystallite size is much smaller, mostly in the sub-micron to single micron range. When X is further increased to 7.5 mol%

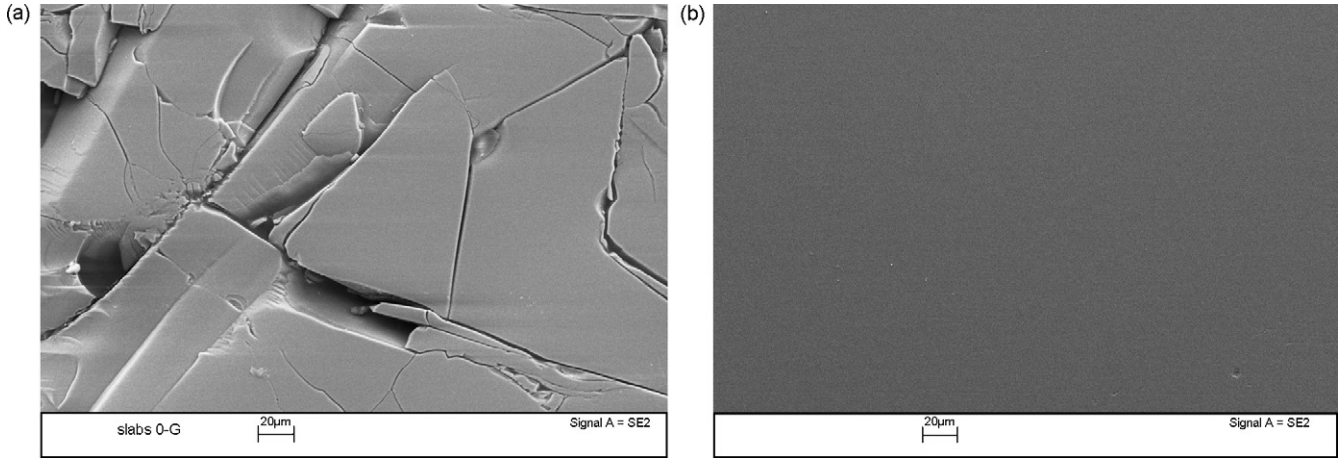

Fig. 5. SEM micrographs of as-quenched glasses: (a) $X = 0.0$ mol% and (b) $X = 10.0$ mol%.

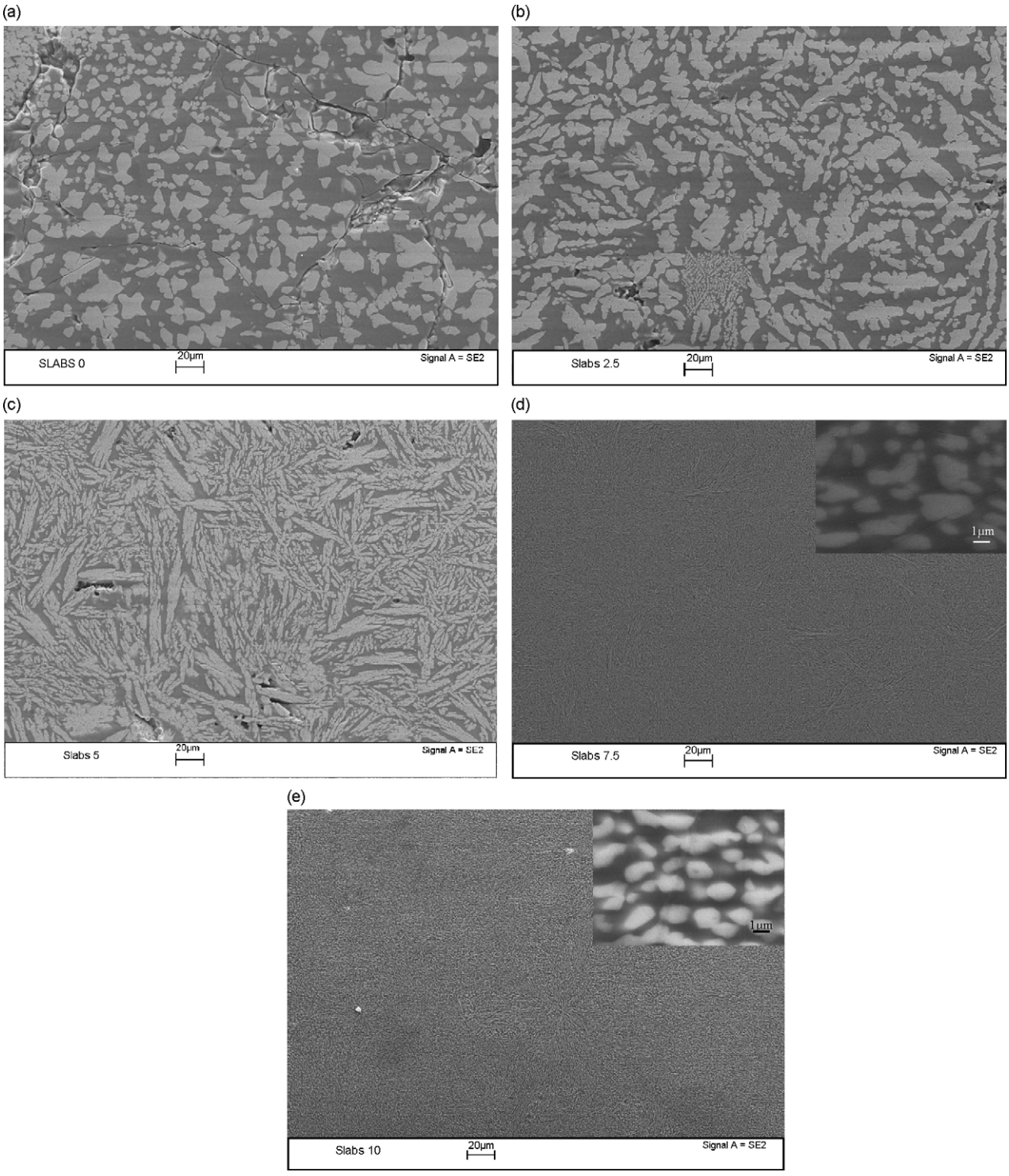

Fig. 6. SEM micrographs of thermally cycled glasses: (a) $X = 0.0$ mol%, (b) $X = 2.5$ mol%, (c) $X = 5.0$ mol%, (d) $X = 7.5$ mol% and (e) $X = 10.0$ mol%.

(Fig. 6(d)) and 10.0 mol% (Fig. 6(e)), the crystallites are only ~1 μm size, still with elongated shape. Sizes of the crystallites for X at 10.0 mol% are smaller than those for X at 7.5 mol%. More importantly, these crystallites uniformly distribute in the glass matrix.

From the SEM observation, it clearly demonstrates that Al_2O_3 is effective in suppressing glass devitrification. This means Al_2O_3 has the function of retaining the vitreous phase in the glass, preventing/delaying a glass matrix with large crystallites, and shifting the glass softening process to higher temperatures. Nevertheless, complete suppression of crystalline phase formation is not possible for the glass compositions studied. Also, Al_2O_3 content cannot be excessively increased for glass forming purpose.

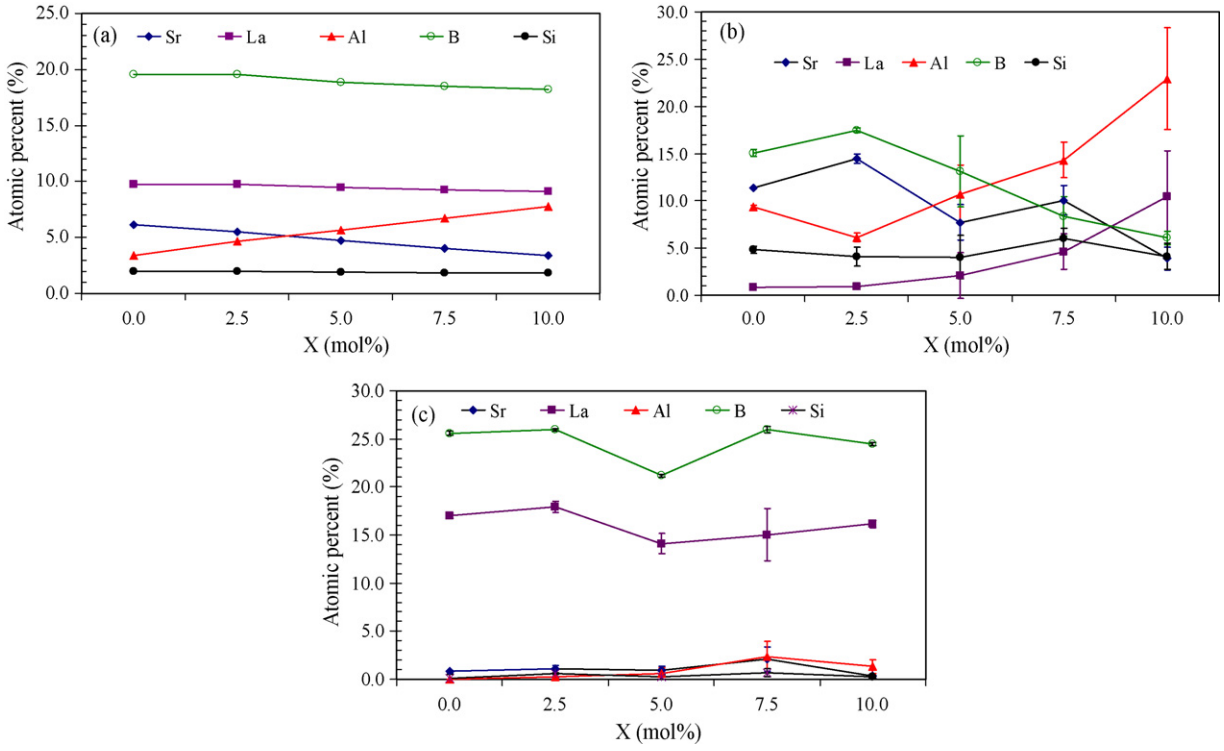

Fig. 7. Comparison of (a) the nominal compositions of the as-quenched glasses, (b) the glass phase compositions and (c) the crystalline phase compositions of the DSC thermally cycled samples.

3.4. Energy dispersive spectroscopy

The results of EDS are shown in Fig. 7 for the designed glass compositions, and the residual glass phase and the crystalline phase of the thermally cycled glasses. With the understanding that the EDS technique is not well suited for absolute quantification of sample compositions, the thermally cycled sample compositions are determined by using the as-quenched glass compositions as standard. The composition analysis obtained by this procedure is very consistent as shown in Fig. 7. The larger standard deviation at high X values is a result of decreasing crystalline size to the detection limit of the EDS technique.

From Fig. 7(a) and (b), it can be seen that the composition of the glass matrix after the thermal cycling is very different from that of the nominal composition of the as-quenched glass. The main difference is the substantially reduced La and B in the glass matrix after the thermal cycling. Significant increase in Sr, Al and Si contents is observed in the residual glass phase. The crystalline phase has the highest percent of B followed by La as shown in Fig. 7(c). Very small amount of Sr is also present. Small amounts of Al and Si concentrations in the crystalline phases are present except for X at 0.0 mol% and 2.5 mol%. The presence of La and B is supported by the $LaBO_3$ phase detected from the XRD patterns. The presence of very small amount of Sr, Al and Si is also detected in the XRD patterns as minor phases.

3.5. X-ray diffraction

The XRD patterns of two as-quenched glass compositions ($X = 0.0$ mol% and 10.0 mol%) and the thermally cycled samples of all the glass compositions are shown in Fig. 8. For the as-quenched samples (Fig. 8(a)), no crystalline phase is detected.

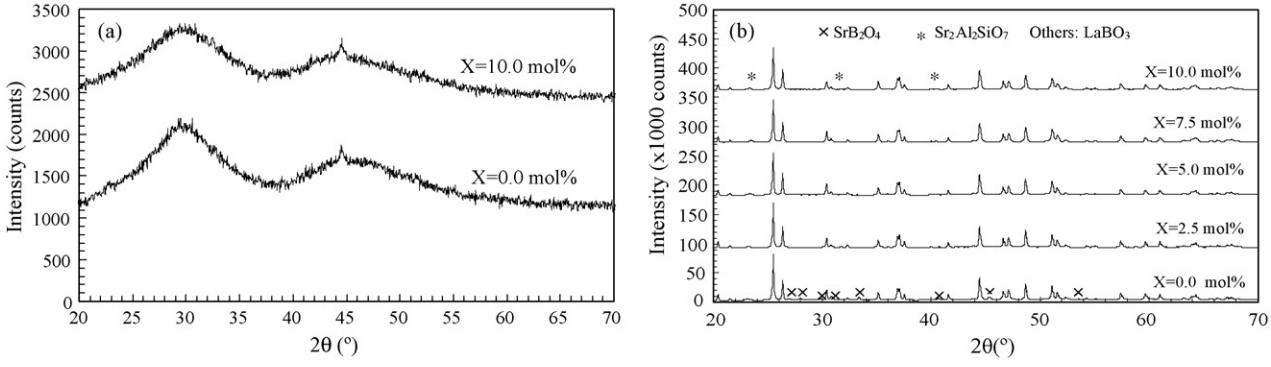

Fig. 8. X-ray diffraction patterns of (a) as-quenched and (b) thermally cycled samples.

Since $X = 0.0$ mol% and $X = 10.0$ mol% cover the two limits of the glass compositions studied, this confirms the SEM observation in Fig. 5 that all the compositions start with pure glass phase. For the thermally cycled samples, devitrification is observed (Fig. 8 (b)). From $X = 0.0$ mol% to 10.0 mol%, orthorhombic $LaBO_3$ is the main crystalline phase. At $X = 0.0$ mol%, small amount of orthorhombic SrB_2O_4 is identified. In other compositions, $Sr_2Al_2SiO_7$ is the minor phase. This observation also supports the EDS result about the presence of small amount of Sr, Al and Si. This means La_2O_3 and B_2O_3 devitrification into $LaBO_3$ is the main process during the thermal cycling. When the Al_2O_3 content is low (at $X = 0.0$ mol%), SrB_2O_4 crystallization cannot be effectively suppressed. SrO participates in devitrification at all conditions but the effect is small.

The devitrification tendency of the studied glass system can be understood from the electrostatic bond strength point of view, even though this explanation might somehow simplify the actual process. The electrostatic bond strength of La^{3+} ion is 0.375 and Sr^{2+} ion is 0.25. La^{3+} tends to separate from the parent glass phase due to its high electrostatic bond strength and bonds with trigonally coordinated B^{3+} to form $LaBO_3$ crystalline phase. Electrostatic bond strength of 0.25 for Sr^{2+} ion is a transition value for silicate glass. However, it can cause borate glass phase separation since B_2O_3 is a weaker glass former [19]. Since the glass compositions contain both B_2O_3 and SiO_2, Sr^{2+} probably plays a minor role in phase separation. This assumption is supported by the presence of SrB_2O_4 crystal phase in minor amount for the composition at $X = 0.0$ mol% and very small amount of Sr^{2+} in Fig. 7(c). Al^{3+} seems to display some unusual behavior. In spite of the potential to have high electrostatic bond strength (0.5 in octahedral coordination and 0.75 in tetrahedral coordination), Al^{3+} tends to be tetrahedrally coordinated in the glass network [20]. This is supported by the enriched Al^{3+} concentration in the residual glass phase and small concentration of Al^{3+} in the crystalline phase in the thermally cycled samples (Fig. 7(b)). Absence of SrB_2O_4 phase and appearance of $SrAl_2SiO_7$ phase in all the compositions except for $X = 0.0$ mol% indicates that there is a critical Al_2O_3 concentration to suppress the formation of SrB_2O_4. From XRD patterns it is also apparent that there is more minor phase in the composition of $X = 0.0$ mol% than in all other compositions. Based on these observations, La_2O_3 and B_2O_3 will be modified in future studies. B_2O_3 change should be made carefully because of its essential role in forming glass and increasing CTE. Although SrO participates in devitrification, reducing SrO will likely decrease CTE as seen from Fig. 4. From EDS and XRD analyses it indicates that Al_2O_3 should be lowered since it decreases CTE (Fig. 4) and forms minor phase at $X = 10.0$ mol%.

4. Conclusions

Seal glasses are synthesized based on $(25 - X)$SrO–$20La_2O_3$–$(7 + X)Al_2O_3$–$40B_2O_3$–$8SiO_2$ system and X has been varied from 0.0 mol% to 10.0 mol%. All the compositions have glass transition temperatures T_g above 620 °C and crystallization temperatures T_c above 826 °C. Also, the glasses have thermal expansion coefficients CTE between $9.0 \times 10^{-6}\,K^{-1}$ and $14.5 \times 10^{-6}\,K^{-1}$ after the first thermal cycle. Suitable increase of Al_2O_3 stabilizes the glass by suppressing devitrification. La_2O_3 and B_2O_3 contribute to devitrification by forming $LaBO_3$. The role of other oxides on the stability of this system is not significant. While this sealant has many desirable properties, future glass composition improvement for stable sealant material will focus on reducing La_2O_3 and B_2O_3.

Acknowledgement

This material is based upon work supported by the Department of Energy under Award Number DE-FC07-06ID14739.

References

[1] S. Elangovan, J.J. Hartvigsen, L.J. Frost, Int. J. Appl. Ceram. Technol. 4 (2007) 109–118.
[2] N.Q. Minh, J. Am. Ceram. Soc. 76 (1993) 563–588.
[3] R.N. Singh, Ceram. Eng. Sci. Proc. 25 (2004) 299–307.
[4] S. Singhal, Am. Ceram. Soc. Bull. 82 (2003) 9601–9610.
[5] S.C. Singhal, K. Kendall, High Temperature Solid Oxide Fuel Cells, Elsevier, Oxford, 2003, p. 217.
[6] R. Draper, S.E. Veyo, US Patent No. 4,801,369 (1989).
[7] J.W. Fergus, J. Power Sources 147 (2005) 46–57.
[8] I.W. Donald, J. Mater. Sci. 28 (1993) 2841–2886.
[9] N.P. Bansal, Ceram. Eng. Sci. Proc. 11 (1990) 1072–1086.
[10] K. Eichler, G. Solow, P. Otschik, W. Schaffrath, J. Eur. Ceram. Soc. 19 (1999) 1101–1104.
[11] K.L. Ley, M. Krumpelt, R. Kumar, J.H. Meiser, I. Bloom, J. Mater. Res. 11 (1996) 1489–1493.
[12] R.E. Loehman, H.P. Dumm, H. Hofer, Ceram. Eng. Sci. Proc. 23 (2002) 699–705.
[13] M.B. Volf, Chemical Approach to Glass, Glass Sci. Tech., vol. 7, Elsevier, New York, 1984, p. 132.
[14] J.H. Jean, T.K. Gupta, J. Mater. Res. 8 (1993) 356–363.
[15] J.E. Shelby, Introduction to Glass Science and Technology, 2nd ed., Royal Society of Chemistry, Cambridge, 2005, p. 159.
[16] S.B. Sohn, S.Y. Choi, G.H. Kim, H.S. Song, G.D. Kim, J. Am. Ceram. Soc. 87 (2004) 254–260.
[17] R.N. Singh, Int. J. Appl. Ceram. Technol. 4 (2007) 134–144.
[18] C. Story, K. Lu, W.T. Reynolds Jr., D. Brown, Int. J. Hydrogen Energy, in press.
[19] S. Block, E.M. Levin, J. Am. Ceram. Soc. 40 (1957) 113–118.
[20] E.M. Levin, S. Block, J. Am. Ceram. Soc. 41 (1958) 49–54.